Palaeomagnetism and K–Ar dating of Cretaceous basalts from Mongolia

Fatim Hankard, Jean-Pascal Cogné, Xavier Quidelleur, Amgalan Bayasgalan, P. Lkhagvadorj

Geophys. J. Int. (2007) **169,** 898–908 doi: 10.1111/j.1365-246X.2007.03292.x

Palaeomagnetism and K–Ar dating of Cretaceous basalts from Mongolia

Fatim Hankard,[1] Jean-Pascal Cogné,[1] Xavier Quidelleur,[2] Amgalan Bayasgalan[3] and P. Lkhagvadorj[3]

[1]*Laboratoire de Paléomagnétisme, Institut de Physique du Globe de Paris & Université Paris* 7, 4 *Place Jussieu,* 75252 *Paris Cedex* 05*, France. E-mail: hankard@ipgp.jussieu.fr*
[2]*Laboratoire de Géochronologie Multi-techniques U.P.S. – I.P.G.P., Bat.* 504*, Sciences de la Terre, Université Paris Sud,* 91405 *Orsay, France*
[3]*Mongolian University of Science and Technology, P.O. Box* 49/418*, Ulaanbaatar* 210349*, Mongolia*

Accepted 2006 November 7. Received 2006 November 7; in original form 2006 May 3

SUMMARY

We report a combined geochronology and palaeomagnetic study of Cretaceous igneous rocks from Shovon (44.4°N, 103.8°E) and Arts-Bogd (44.3°N, 102.2°E) localities in the Gobi Desert, south Mongolia. K–Ar dating based on seven rock samples, with two independent measurements for each sample, allows us to propose an age of 94.7 ± 1.3 Ma for Shovon locality and a 98.2 ± 1.4 to 118.3 ± 1.7 Ma age range for Arts-Bogd. Stepwise thermal and AF demagnetization generally isolated a high temperature component (HTC) of magnetization for both Shovon and Arts-Bogds basalts, eventually following a low temperature component (LTC) in some samples. The HTC directions display normal polarity, consistent with the Cretaceous Long Normal Superchron. Rock magnetic analysis identifies fine-grained pseudo-single domain (PSD) magnetite and titanomagnetite as primary carriers of the remanence. Mean HTC palaeomagnetic direction is Dm = 8.2°, Im = 63.7° ($n = 18$ flows, $k = 41.1$, $\alpha_{95} = 5.5°$) for Shovon and Dm = 12.1°, Im = 66.4° ($n = 27$ flows, $k = 53.0$, $\alpha_{95} = 3.9°$) for Arts-Bogd. Because of their similar ages, we combine data from Shovon and data previously obtained from Khurmen Uul (92.0 ± 4.0 Ma), recomputed in geographic coordinates, and not in tilt-corrected ones as in our previous interpretation, at the Shovon locality. The combined final average palaeomagnetic direction for Shovon-Khurmen Uul is Dm = 7.4°, Im = 62.7° ($n = 23$ flows, $k = 41.4$, $\alpha_{95} = 4.8°$). The corresponding palaeopoles computed from these HTC lie at $\lambda = 84.7°$N, $\phi = 195.0°$E, $dp/dm = 5.8/7.5$ for Shovon-Khurmen Uul (average age: 93.4 ± 2.6 Ma) and $\lambda = 80.5°$N, $\phi = 159.0°$E, $dp/dm = 5.2/6.3$ for Arts-Bogd (average age: 104.6 ± 6.6 Ma). These poles are consistent with those from the European apparent polar wander path (APWP) at 90, 100 and 110 Ma, and other published pole from the Mongol-Okhotsk suture zone, Amuria and North China blocks. This confirms the lack of a discernable latitudinal motion between Amuria and Siberia since their final accretion by the Late Jurassic–Early Cretaceous, and reinforces the idea that Europe APWP can be used as a reference for Siberia by the mid-Cretaceous. We finally propose a mid-Cretaceous mean palaeomagnetic pole for the Siberia-Amuria-North China Block assemblage which lies at: $\lambda = 86.4°$N, $\phi = 191.1°$E ($n = 10$, $k = 74.9$, $A_{95} = 5.8°$).

Key words: basalts, Cretaceous, Mongolia, K–Ar dating, palaeomagnetism.

1 INTRODUCTION AND SAMPLING

Central Asia is a fascinating place for testing palaeomagnetic tools that provide for tectonic constraints. In effect, because the India plate is continuously penetrating into Eurasia since its collision at ∼50 Ma (e.g. Molnar & Tapponnier 1975; Tapponnier & Molnar 1979; Patriat & Achache 1984), it causes the Eurasian continent to deform. This deformation is accommodated by two main components of (1) east and southeastward extrusions of continental lithospheric units (Fig. 1) or blocks (Tapponnier *et al.* 1986) such as the Indochina block (Yang & Besse 1993) or Amuria block (Halim *et al.* 1998a; Cogné *et al.* 2005) and (2) northward convergence of Central Asian blocks with respect to Siberia since the onset of collision (e.g. Enkin *et al.* 1992; Chen *et al.* 1993; Halim *et al.* 1998b). Palaeomagnetism is sensitive to inclination, therefore, it is a powerful tool to describe these northward versus southward palaeolatitude movements between different blocks. For this reason, numerous palaeomagnetic studies have been undertaken

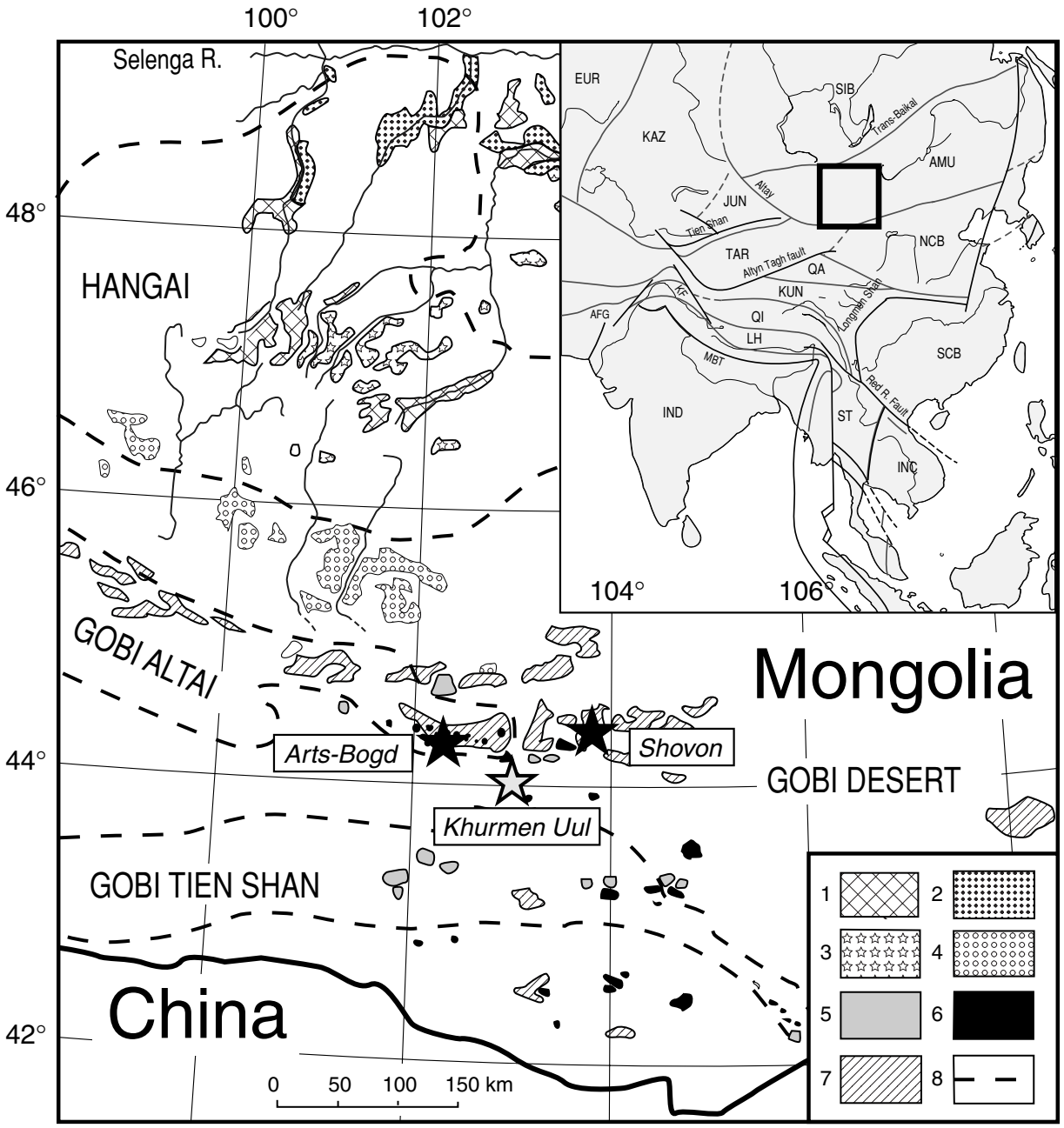

Figure 1. Simplified map of Late Mesozoic–Cenozoic volcanic fields in Southern and Central Mongolia (after Kovalenko *et al.* 1997). Black stars: Shovon (94.7 ± 1.3 Ma), and Arts-Bogd (98.2 ± 1.4–118.3 ± 1.7 Ma) localities; light grey star: Khurmen Uul (92.0 ± 4.0 Ma) locality (Hankard *et al.* 2005); *Legend*: (1) Pleistocene-Holocene; (2) Pliocene; (3) Middle Miocene; (4) Late Oligocene and early Miocene; (5) Early Cenozoic; (6) Late Cretaceous; (7) Late Jurassic and Early Cretaceous and (8) Boundaries of highlands and ranges. *Inset:* situation map of studied area in Asia, with main blocks and limits indicated (AMU: Amuria, AFG: Afghanistan, EUR: Eurasia main plate, INC: Indochina, IND: India JUN: Junggar, KAZ: Khazakhstan, KF: Kunlun Fault, KUN: Kunlun, LH: Lhasa, MBT: Main Boundary Thrust, NCB: North China Block, QA: Qaidam, QI: Qiangtang, SCB: South China Block, SIB: Siberia, ST: Shantaï, TAR: Tarim).

all-over Asia in the last 25 yr. They all show that (pre-collision) Cretaceous palaeomagnetic poles from Central Asian blocks (e.g. Lhasa, Qiangtang, Kunlun, Qaidam, Tarim and Junggar; Fig. 1) are far-sided from the Europe Apparent Polar Wander Path (APWP) as defined by Besse and Courtillot (Besse & Courtillot 1991, 2002, 2003) when considered at site locations (e.g. Chen *et al.* 1993; Halim *et al.* 1998b).

This analysis, however, has been, until recently, based on the Cretaceous part of a reference APWP that does not rely on palaeomagnetic data from the easternmost parts of the Eurasian continent. Therefore, there was a need to check for the validity of the Cretaceous part of Eurasian APWP as a reference for describing convergence between Siberia and southernmost Central Asian blocks. Recently, some studies (Kravchinsky *et al.* 2002; Cogné *et al.* 2005) have demonstrated the Late Jurassic/Early Cretaceous closure of the Mongol-Okhotsk ocean, confirming that Siberia, Amuria and North China Block (NCB) should have formed a single entity since that time.

Following Zonenshain *et al.* (1990), the Amuria microcontinent consists of a number of lithospheric blocks (Hangai, Hentei, Central Mongolia, Argun and Khingan-Bureya), which accreted together in the early Palaeozoic. Numerous palaeomagnetic studies showed that (1) NCB accreted to Amuria by the Late Carboniferous, (2) South China Block (SCB) then sutured with NCB around the Middle to Late Jurassic and (3) the final suturing between Amuria and Siberia was achieved by the Late Jurassic–Early Cretaceous with the closure of the Mongol-Okhotsk ocean (e.g. Zhao & Coe 1987; Zhao *et al.* 1990; Chen *et al.* 1993; Ma *et al.* 1993; Gilder *et al.* 1996; Gilder & Courtillot 1997; Halim *et al.* 1998a; Yang *et al.* 2001; Yang & Besse 2001; Kravchinsky *et al.* 2002; Cogné *et al.* 2005). The Amuria block is a key region for understanding the transition between the Tarim and Jungar basins to the west, which exhibit significant post-Cretaceous convergence, and the Siberia craton (e.g. Chen *et al.* 1992; Gilder *et al.* 2003). However, apart from the study of Pruner (1992), no Cretaceous data were yet available from within the interior of Amuria block, between the northern edge of Amuria block (Fig. 1) and NCB in the mid-Cretaceous.

With the aim of enlarging this dataset, we undertook a series of palaeomagnetic and geochronology sampling in Cretaceous basaltic formations from the Gobi desert in Mongolia (Fig. 1) in the summers of 1999 and 2004. We focussed our sampling on effusive formations in order to (1) have good opportunities to date the sampled rocks and (2) avoid possible inclination shallowing processes which may occur in sediments. We present the results of two new localities (Fig. 1). We collected 164 cores at 20 sites (19 flows) from the Shovon locality (44.3°N, 103.8°E), and 282 cores at 34 sites (32 flows or necks) from the foothills of the Arts-Bogd range (e.g. Whitford-Stark 1987) (44.4°N, 102.2°E; Arts-Bogd locality hereafter). In both localities flows are flat lying, or display slight tilts, lower than 10°, which are likely resulting from flow emplacement. This is confirmed by field observations of the underlying Cretaceous redbeds we observed at some locations in Arts-Bogd that are flat lying as well. We thus conclude that no significant tectonic tilts affect these flows and volcanic edifices. In both localities, volcanoes and flows are distributed over a fairly large area ($\sim 20 \times 20$ km), which precludes any clear stratigraphic relationships from being established between the outcrops. Finally, we also collected hand-samples for geochronological dating from several of the palaeomagnetic sampling sites. In the following, we first present methods and results of our radiochronological datings, and then the results obtained from palaeomagnetic analyses.

2 GEOCHRONOLOGICAL METHOD AND RESULT

K–Ar dating was conducted in the Geochronology Multi-techniques U.P.S.–I.P.G.P. laboratory at the University of Orsay, France, using the Cassignol-Gillot technique (Cassignol & Gillot 1982). For each hand sample collected in the field, about 1–2 kg of fresh rock were crushed and then sieved to a 100–250 μm size fraction. Crushed samples were cleaned with deionised water. In order to remove possible traces of weathered material, the crushed samples were again cleaned in a 5 per cent nitric acid solution for 15 min in an ultrasonic bath. Phenocrysts and weathered phases were carefully removed using the heavy liquids, diiodomethane and bromoforme, to minimize the occurrence of extraneous ^{40}Ar contamination. This mineralogical separation allowed us to access microlitic groundmass within a narrow density range, typically between 2.95 and 3.00 g cm^{-3}. The groundmass is chosen because of its higher K content and also because it crystallized at the surface following eruption and, therefore, is the most likely phase to have equilibrated with the atmosphere. Potassium was measured by flame emission spectrometer and was compared with reference values from the MDO-G and ISH-G standards (Gillot *et al.* 1992). Between 80 and 300 mg of sample was wrapped in Cu foil and progressively fused for 45 min up to 1500 °C using a high-frequency furnace. This temperature allows a complete extraction of argon from the basaltic groundmass. Before analysis in the mass spectrometer, the gas underwent multiple-step cleaning using Ti foam at 700 °C and SAES MP-10 getters at 400 °C. The obtained clean argon gas was analysed using the K–Ar Cassignol-Gillot technique (Cassignol & Gillot 1982). This method is based on a double isotopic comparison between atmospheric argon and argon extracted from the sample using a mass spectrometer identical to the one described by Gillot & Cornette (1986). The ^{40}Ar signal calibration is performed prior to each analysis using a 0.1 cm^3 air pipette calibrated by volumetric determination and by repeated analyses of an interlaboratory standard GL-O with a recommended value of 6.679×10^{14} at g^{-1} of ^{40}Ar*. (Odin *et al.* 1982). Typical uncertainties of 1 per cent are reached for ^{40}Ar calibration and K content measurement. The detection limit of the system is 0.1 per cent of ^{40}Ar* (Quidelleur *et al.* 2001). Ages were calculated using the decay constants proposed by Steiger & Jaeger (1977). Analyses were duplicated and yielded a concordant value at the 1σ level in most cases, except samples MO-153 and MO-118, which were duplicated at the 2σ level. The mean ages and uncertainties have been obtained by weighted each duplicate by their radiogenic content.

Table 1 reports the seven new age determinations calculated from fourteen K–Ar analyses. At the Shovon locality, age determinations for two hand-samples from different flows provide exactly the same ages of 94.7 ± 1.3 Ma. In contrast, the five random sites we have sampled for K–Ar dating at Arts-Bogd, amongst 34 different volcanic edifices, necks and lava flows, display a larger age distribution ranging from 98.2 ± 1.4 to 118.3 ± 1.7 Ma (Table 1). Moreover, these ages are drastically different from the 47 Ma, obtained from whole rock K–Ar and reported in literature without analytical details, for this area (Whitford-Stark 1987; Yarmolyuk *et al.* 2002). We finally note that all our dates fall into the Cretaceous Long Normal Superchron (CLNS), implying an expected normal polarity for our palaeomagnetic results (Cande & Kent 1995; Gradstein *et al.* 2004).

3 PALAEOMAGNETIC ANALYSIS

In general, eight standard 2.5-cm-diameter cores were drilled at each site using a gasoline powered portable drilling machine and oriented with magnetic and Sun compasses, in order to check and correct for local declination anomalies. For samples for which sun compass orientation was not measured, because of cloudy weather, we used the IGRF 2000 coefficients to correct for local magnetic deviation. The local magnetic deviations computed from comparison of magnetic and solar azimuths are $-1.2° \pm 2.7°$ and $-1.6° \pm 3.6°$ for Shovon and Arts-Bogd, respectively. These values are consistent with the declinations computed for the summer 2004 from the IGRF 2000 coefficients and their time derivatives in the Shovon ($-2.0°$) and Arts-Bogd ($-1.3°$) areas.

In the Palaeomagnetic laboratory of the Institut de Physique du Globe de Paris (IPGP), the cores were cut into 2.2-cm-long specimens. These samples were subjected to stepwise thermal and alternating field (AF) demagnetizations. Samples were heated and

Table 1. K-Ar ages of basalts from the Shovon and Arts-Bogd areas (Gobi Desert, Mongolia).

				Radiogenic ^{40}Ar				
Locality	Sample name	Range of crystal sizes (μm)	K %	% ^{40}Ar*	^{40}Ar* (at/g)	Age $\pm1\sigma$ (Ma)	Mean age $\pm1\sigma$ (Ma)	Polarity
Shovon	MO-155	125–250	1.49	94.0	1.5020*E*+14	94.2±1.3	94.7±1.3	N
				91.9	1.5200*E*+14	95.3±1.4		
Shovon	MO-153	125–250	1.76	92.6	1.7475*E*+14	92.5±1.3	94.7±1.3	N
				94.0	1.8306*E*+14	96.8±1.4		
Arts-Bogd	MO-118	125–250	1.58	80.3	1.6372*E*+14	96.8±1.4	98.2±1.4	N
				78.5	1.6889*E*+14	99.7±1.4		
Arts-Bogd	MO-116	100–200	1.78	65.5	1.9222*E*+14	100.3±1.4	100.4±1.4	N
				84.4	1.9253*E*+14	100.4±1.4		
Arts-Bogd	MO-101	100–200	2.41	93.1	2.6261*E*+14	101.4±1.4	101.9±1.4	N
				90.3	2.6494*E*+14	102.3±1.5		
Arts-Bogd	MO-109	125–250	1.84	85.0	2.0729*E*+14	104.6±1.5	103.7±1.5	N
				87.1	2.0344*E*+14	102.8±1.5		
Arts-Bogd	MO106	100–200	1.15	43.5	1.4670*E*+14	118.4±1.7	118.3±1.7	N
				54.4	1.4651*E*+14	118.2±1.7		

Note: K: percent of K; ^{40}Ar* (%): percent of radiogenic ^{40}Ar; ^{40}Ar* (at/g): number of atoms of radiogenic ^{40}Ar per gram; Age: K-Ar age; 1σ: age uncertainty; N: normal polarity of magnetic field.

cooled within a nearly zero field laboratory-built furnace at IPGP. Magnetic measurements and demagnetization procedures were performed in a magnetically shielded room. Remanent magnetization measurements were carried out using Agico JR5 and JR6 spinner magnetometers. During thermal demagnetization, sample orientation was successively inverted about the *z*-axis in order to detect any systematic magnetization that could have resulted from the small ($\sim$10 nT) residual magnetic field in the furnace. Changes in magnetic mineralogy during thermal demagnetization were monitored by measurements of magnetic susceptibility after each heating step using a KLY-2 susceptibility-meter. In order to better constrain the magnetic mineralogy and assist in the identification of the magnetic carriers, rock magnetism involving acquisitions of isothermal remanent magnetization (IRM) were performed on a few selected specimens. Hysteresis loops were also determined on a few specimens, using a laboratory-made translation inductometer. Determinations of Curie points were carried out with Kappa-bridge KLY-3 and CS-2 high temperature susceptibility meters. Changes in the intensity and direction of remanent magnetization vectors during demagnetization processes were analysed using vector-end-point projections (Zijderveld 1967). The magnetic directions were identified using principal component analysis (Kirshvink 1980) or remagnetization great circle methods (Halls 1978; McFadden & McElhinny 1988). Site-mean directions were calculated using Fisher statistics (Fisher 1953), or using the statistics of McFadden & McElhinny (1988) for combined directional data and remagnetization circles. All interpretations and data processing were carried out using the PalaeoMac software (Cogné 2003).

3.1 Results from Shovon region

The intensity of natural remanent magnetization (NRM) of basalt samples of Shovon locality varies from 0.4 to 9.6 A m^{-1} with an average value at 2.3 $\pm$ 1.5 A m^{-1}, except for sites 158 and 159. Specimens from these two latter sites show intensity ranging from 11 to 55 A m^{-1} (up to 74 A m^{-1} for a specimen from site 159), with a mean value at 23.2 $\pm$ 20.3 A m^{-1}. The calculation of Koenigsberger (1938) ratios gives values of 4.0 for site 158 and 11.2 for site 159, whereas the average value obtained from 10 sites (from sites 149–157 and 160) amounts to 0.8 $\pm$ 0.5. Specimens from sites 158 and 159 most likely carry an isothermal remanent magnetization (IRM) due to lightning. This component is easily removed below the 250–350 °C temperature range.

Representative examples of magnetization behaviour during thermal and AF demagnetization are shown in Figs 2(a) and (b). Thermal and AF demagnetization of specimens allowed us to isolate one single magnetization component in most cases. In general, this well-defined high temperature component (HTC) converges towards the origin and unblocks between 235 °C and 590–600 °C or in a peak field from 4 to 100 mT. Such is not the case for all the specimens from sites 141, 153 and 156 where some low temperature components (LTC) were poorly separated from HTC, leading to a great-circle path of points. In site 141, the HTC was well separated in six out of seven samples, only three out of five samples from site 153, and finally five out of seven samples from site 156. Site-mean directions (Table 2) of these three sites were thus computed using the combined average of McFadden & McElhinny (1988). In contrast, only remagnetization great-circles could be defined in sites 154 and 159. In these sites, we computed an average remagnetization great circle, using the bivariate statistics of Le Goff (1990).

The maximum unblocking temperature together with rock magnetism experiments indicate that magnetite is the dominant carrier of the magnetic remanence for these volcanic rocks. A typical example of a hysteresis loop (Fig. 2c) shows that the sample is saturated after applying a field at 0.3–0.4 T. This is corroborated by the high temperature susceptibility measurement that exhibits a sharp drop of susceptibility around 580 °C, close to the Curie point of magnetite (Fig. 2d). These observations confirm that HTC is carried by magnetite and most likely represents the primary magnetization for these 18 basaltic lava flows.

The combined site-mean directions of HTC and great circles are listed in Table 2 and illustrated on an equal-area projection of Fig. 3. Directions (black dots) exhibit a single normal polarity magnetization, which is consistent with the age of flow-emplacement within the CLNS. According to field observations, lava flows occurred subhorizontaly and volcanic edifices and necks appeared subvertical.

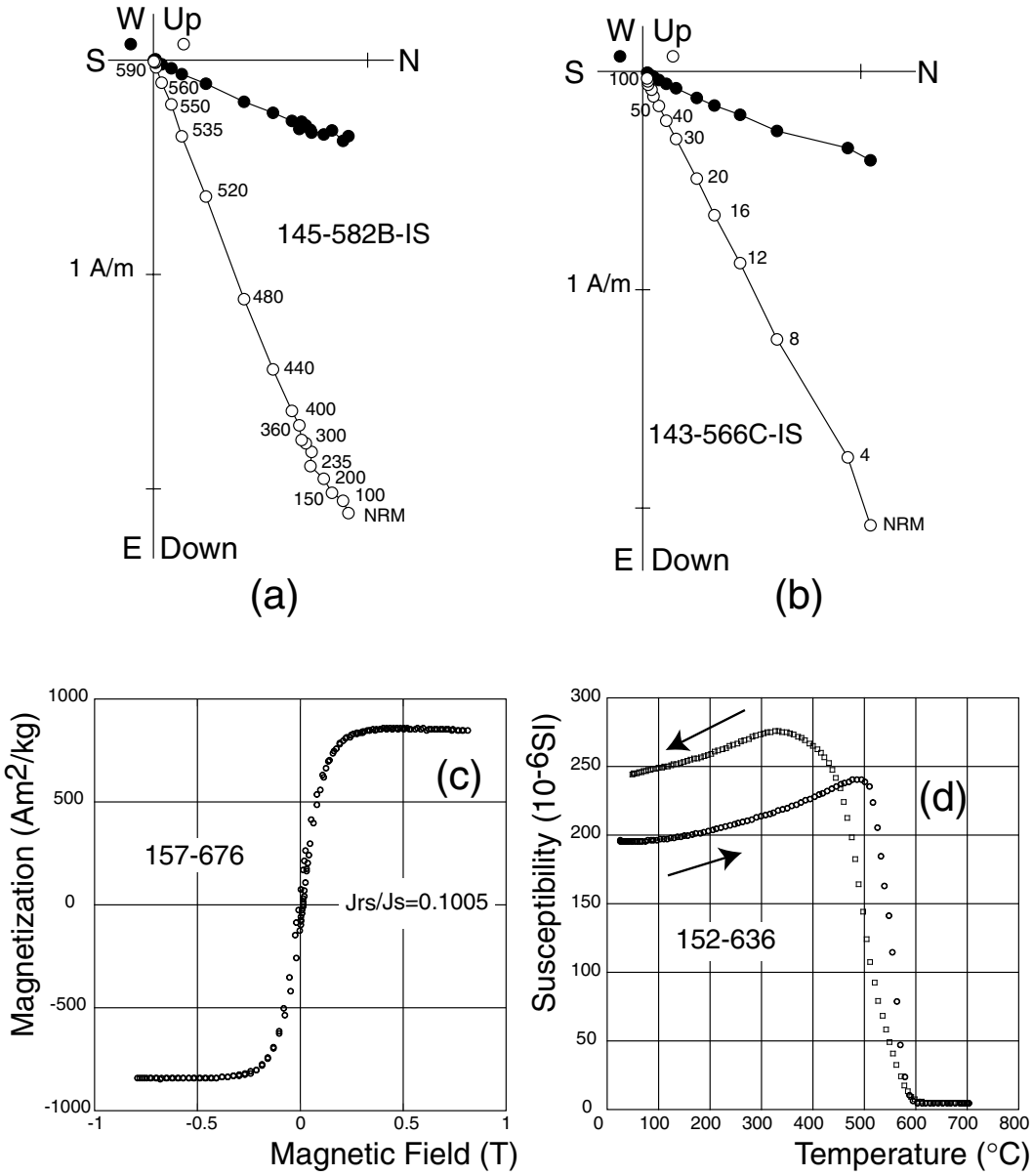

Figure 2. Thermal and alternating field (AF) demagnetization and rock magnetism experiments for the Shovon locality: (a) & (b): Typical examples of orthogonal vector plots (Zijderveld 1967) in geographic coordinates during thermal (a) and AF (b) demagnetizations showing single magnetization component behaviour; Solid (open) symbols are projections onto the horizontal (vertical) plane; temperature steps are indicated in °C, alternating field in mT; (c): Hysteresis loop after the correction of the paramagnetic component showing the presence of a low-coercivity magnetic mineral and (d) High temperature susceptibility measurements curve showing a Curie point around 580 °C; temperatures are indicated in °C; Arrows indicate heating or cooling.

We therefore, interpret the very slight local dips we observed as being original and probably not linked to tectonics. We therefore, assume that no tilt correction is required for this locality. Excluding the mean great circle from site 154 which is clearly an outlier, the combined final mean palaeomagnetic direction of the 18 flows is $D = 8.2^\circ$, $I = 63.7^\circ$ ($n = 18$, $k = 41.1$, $\alpha_{95} = 5.5^\circ$; Table 2), in geographic coordinates.

3.2 Combined Shovon-Khurmen Uul mean palaeomagnetic directions

In a previous study (Hankard *et al.* 2005), we presented the palaeomagnetic results obtained from 6 basaltic lava flows from Khurmen Uul locality dated at 92.0 ± 4.0 Ma (Yarmolyuk *et al.* 1995). We propose, because of (1) the small number of flows in Khurmen Uul, (2) its proximity to the Shovon locality (44.0°N/103.0°E and 44.4°N/103.8°E, representing a distance of ∼80 km) and (3) their similar ages (92.0 ± 4.0 Ma versus 94.7 ± 1.3 Ma), to compute a palaeomagnetic mean direction, for an average age of 93.4 ± 2.6 Ma, by combining the results from both studies. To this purpose, we have recomputed individual *in situ* flow-mean directions of Khurmen Uul (Hankard *et al.* 2005) at the Shovon locality (Table 2).

We also reconsider our analysis of Khurmen Uul results. In effect, because flow mean directions from Khurmen Uul clustered upon the tilt-correction, we assumed (Hankard *et al.* 2005) that the overall direction in tilt-corrected coordinates probably represented the magnetic direction at the time of flow emplacement. The

Table 2. Site-mean paleomagnetic direction for high temperature component (HTC) of Upper Cretaceous effusives from Shovon, Khurmen Uul and Arts-Bogd regions.

Id/Flow	Type	n/N	Dg (°)	Ig (°)	k	α_{95}
Shovon (44.4°N, 103.8°E) – 94.7±1.3 Ma						
141	HT+GC	7/7	357.6	42.4	201.7	4.3
142–144	HT	12/12	32.4	65.1	177.8	3.3
143	HT	4/6	30.3	60.8	832.6	3.2
145	HT	4/6	23.5	67.8	1146.8	2.7
146	HT	6/6	17.2	69.2	1579.7	1.7
147	HT	5/5	4.3	81.0	403.4	3.8
148	HT	5/5	8.4	77.1	765.1	2.8
149	HT	6/6	312.1	63.3	323.4	3.7
150	HT	5/6	26.1	68.7	494.8	3.4
151	HT	4/5	18.5	63.4	1234.7	2.6
152	HT	5/5	11.8	59.5	392.2	3.9
153	HT+CG	5/5	17.3	57.0	236.4	5.4
154*	GCm	6/6	5.7	59.1	-	6.0
155	HT	3/4	.8	51.0	723.3	4.6
156	HT+CG	5/7	354.9	52.5	116.8	7.3
157	HT	5/6	355.7	55.5	288.5	4.5
158	HT	5/6	21.0	59.7	602.9	3.1
159	GCm	4/5	257.9	1.0	-	16.0
160	HT	5/5	17.6	66.7	300.0	4.4
Mean Shovon		*18/19*	*8.2*	*63.7*	*41.1*	*5.5*
*Khurmen Uul (44.0°N, 103.0°E) – 92.0±4.0 Ma***						
25	HT	10/10	4.3	56.1	154.4	3.9
26–27	GCi	5/20	7.2	59.7	-	5.3
30	HT	8/8	6.6	71.5	46.6	8.2
31–33	HT	15/15	338.9	52.6	39.0	6.2
34	HT	10/10	27.9	49.6	406.1	2.4
Mean Khurmen Uul		*5/5*	*5.1*	*59.0*	*38.8*	*12.4*
Mean Shovon-Khurmen Uul		*23/24*	*7.4*	*62.7*	*41.4*	*4.8*
Arts-Bogd (44.3°N, 102,2°E) – 98.2±1.4 Ma to 118.3±1.7 Ma						
95*	HT+GC	3/6	278.8	72.9	6721.6	2.3
96	HT	3/6	37.3	64.5	520.7	5.4
97*	GCm	4/6	250.5	-23.7	-	4.3
98*	HT	6/6	59.5	-23.7	59.8	8.7
99	GCm	4/6	216.2	13.3	-	6.6
100*	HT	6/6	228.3	15.8	354.8	3.6
101*	HT	6/6	260.6	44.8	156.2	5.4
102	HT	4/6	14.0	61.8	652.3	3.6
103	HT	6/6	351.5	66.9	297.5	3.9
104	HT	5/6	342.1	71.9	353.9	4.1
105–106	HT	11/12	359.5	63.3	160.3	3.6
107	HT	6/6	17.6	77.9	108.5	6.5
108	HT	6/6	18.8	79.3	57.8	8.9
109	HT	5/6	23.4	63.7	902.6	2.5
110	HT	5/6	22.8	58.1	134.6	6.6
111	HT	6/6	2.0	57.5	287.8	4.0
112	HT	5/6	9.8	61.2	435.0	3.7
113	HT	4/4	345.9	48.9	304.1	5.3
114	HT	6/6	349.2	56.7	58.5	8.8
115	HT	5/6	29.7	66.7	96.2	7.8
116	HT+GC	6/6	354.9	70.1	65.2	8.7
117–118	HT	11/12	30.3	52.2	250.0	2.9
119	HT	6/6	55.5	66.7	189.9	4.9
120	HT	4/6	31.2	75.3	407.2	4.6
121	HT	6/6	19.4	51.7	34.1	11.6
122	HT	6/6	23.7	59.7	171.0	5.1
123	HT+GC	4/6	343.1	82.8	429.3	5.2
124	HT+GC	6/6	9.1	67.5	390.9	3.6
125	HT	3/4	15.0	69.0	2172.1	2.6
126	HT	4/4	12.6	66.8	1862.8	2.1
127	HT	6/6	9.7	72.6	335.6	3.7
128	HT	4/4	8.1	61.5	75.3	10.7
Mean Arts-Bogd		*27/32*	*12.1*	*66.4*	*53.0*	*3.9*

Note: HT: high temperature magnetization component;
GC: remagnetization great circle; GCm: normal to average great-circle
GCi: great-circles intersection;
n/N: number of samples used in the statistics/number of demagnetized specimens; Dg/Ig: declination/inclination in geographic coordinates; k, α_{95}: parameters of Fisher Statistics (Fisher, 1953); (*): Flow excluded from the final average calculation; (**) Khurmen Uul data after (Hankard *et al.* 2005), recomputed at the locality of Shovon.

corresponding palaeopole displayed an offset of ∼10° in palaeolatitude with respect to the corresponding reference APWP pole at 90 Ma for Europe (Besse & Courtillot 2002). This caused problems for interpretation because the Amuria block is thought to have accreted on to Siberia by the Late Jurassic–Early Cretaceous, and has not undergone any relative northward movement since then (e.g. (Cogné *et al.* 2005). Our field notes indicate that any tilts of Khurmen Uul flows could be original, therefore, we now propose to use the mean site-directions of this formation in geographic coordinates, rather than in tilt-corrected ones, as previously used. As a matter of fact, when considered in geographic coordinates, the Khurmen Uul site-mean directions (grey triangles, Fig. 3) do not reveal any statistical difference (at the 95 per cent probability level) to those from the Shovon area, where our field observations show that all the flows are generally flat-lying.

We conclude that these directions are statistically indistinguishable from one another, and propose a new mean direction for the

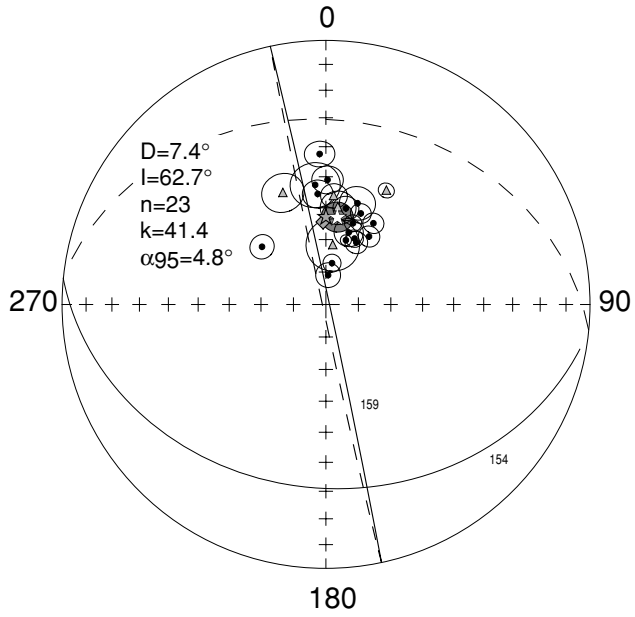

Figure 3. Equal-area projection of HTC site-mean directions with their α_{95} circles of confidence; black solid dots: site-mean directions from Shovon locality; Grey triangle: site-mean directions from Khurmen Uul locality; bold (light) continuous line: site 159 (154) average remagnetization great-circle; white star with shaded α_{95} area: overall-mean direction from Shovon-Khurmen Uul area; solid (open) symbols: positive, downward (negative, upward) inclinations (except for star); grey diamond (star): International Geomagnetic Reference Field (Dipolar Field) direction.

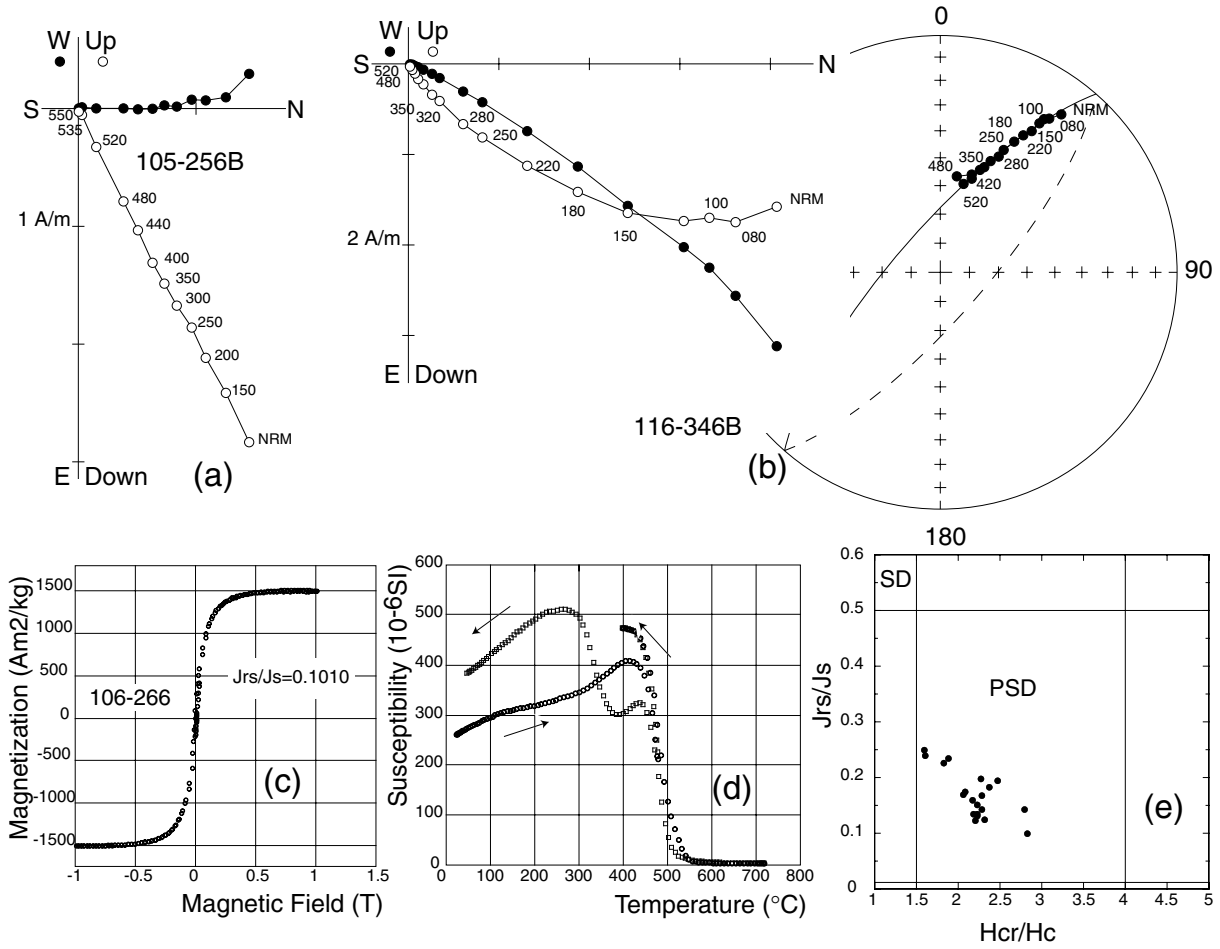

Figure 4. Thermal demagnetization and magnetic mineralogy experiments results from the Arts-Bogd locality; (a) Orthogonal vector plots (Zijderveld 1967), in geographic coordinates; (b) Orthogonal vector plot and stereonet of a specimen from site 116 showing a great-circle path during demagnetization. (c) Hysteresis loop after the correction of the paramagnetic component showing the presence of low-coercivity magnetic mineral; field in Tesla (T); (d) Susceptibility curve versus temperature showing a Curie point at 550 °C; (e) Day (1977) plot showing all samples in the pseudo-single domain (PSD) grain size area. Same conventions as in Fig. 2.

Shovon-Khurmen locality, which supersedes our previous study based only on six flows from Khurmen Uul (Hankard *et al.* 2005). This leads to a new average palaeomagnetic direction, (Table 2, Fig. 3) based on 23 distinct flows, of $D = 7.4°$, $I = 62.7°$ ($n = 23$, $k = 41.4$, $\alpha_{95} = 4.8°$). We have checked for the recording of secular variation by estimating the angular dispersion of virtual geomagnetic poles (VGP) based on the 22 distinct flows (excluding the great-circle), following McFadden *et al.* (1991). We obtain a VGP scatter of 17.0°, which falls within the range (14.9°–19.5°) of VGP scatter predicted at 40–50° latitude during the 80–110 Ma period (McFadden *et al.* 1991). This suggests that the overall mean direction of HTC from our 23 basalt flows from Shovon and Khurmen Uul has fully averaged out the secular variation by the time of flow-emplacements. Although the mean direction contains the Present Earth Field direction (grey star and diamond in Fig. 3), and because of the stability of remenence magnetization, we conclude that the final mean direction is likely to represent the Late Cretaceous time-averaged palaeomagnetic field direction at 93.4 ± 2.6 Ma.

3.3 Results from Arts-Bogd region

In this locality, 198 specimens were subjected to stepwise thermal demagnetization up to a maximum temperature of 590 °C. Most of the samples yielded a stable high temperature magnetization component (HTC) (Fig. 4a). This HTC is generally obtained after removal of a small magnetization of viscous or weathering origin by 80–200 °C, and generally vanishes by 550 °C. This stable HTC was resolved in 96 per cent of the treated samples (190 specimens out of 198) using principal component analysis (Kirshvink 1980). The eight remaining specimens exhibited an overlap of HTC and LTC demagnetization temperature spectra, thus leading to great-circle trajectories (Fig. 4b). Such behaviour is observed for two specimens from sites 95, 116 and 123, three samples from site 124 and four specimens from sites 97 and 99. The characteristic HTC of these samples was resolved using the remagnetization great-circle method. For this reason, the site-mean direction of sites 95, 116, 123 and 124 was computed using the combined average direction of vectors and planes (McFadden & McElhinny 1988), and an average great-circle was computed using the bivariate statistics of Le Goff (1990) at sites 97 and 99 (Table 2).

The maximum unblocking temperature of HTC around 550 °C indicates that titanomagnetite with varying content of titanium is most likely the dominant magnetic carrier in these basalts. Rock magnetism experiments corroborate this observation. A typical example of a hysteresis loop (Fig. 4c) shows that saturation is rapidly achieved after applying a field around 0.3T, thus pointing out the presence

Table 3. Selected Cretaceous paleomagnetic poles from Asia and reference APWP poles for Europe.

Block	Name	Age	Slat	Slon	Plat	Plon	dp/dm or A_{95}	References
Europe APWP		90 Ma	-	-	82.2	202.1	5.2	(*Besse and Courtillot*, 2002;
		100 Ma	-	-	81.7	180.1	6.7	*Besse and Courtillot, 2003)*
		110 Ma	-	-	80.0	183.6	4.2	”
		120 Ma	-	-	78.2	189.4	2.4	”
NCB+SCB	1. NCB+SCB		35.0	110.0	78.0	190.2	3.3	(*Halim et al.*, 1998b)
Siberia	2. Ingoda	K1	51.2	112.2	58.5	176.8	5.2/6.0	(*Cogné et al.*, 2005)
	3. Bichura	K1	50.6	107.6	37.0	70.4	15.8/17.5	”
Amuria	4. Shovon-Khurmen uul	93.4±2.6 Ma	44.4	103.8	84.7	195.0	5.8/7.5	This study
	5. Arts-Bogd	98.2–118.3 Ma	44.3	102.2	80.5	159.0	5.2/6.3	”
	6. Kremljevka	K1	51.8	117.5	86.8	61.8	6.8/7.9	(*Cogné et al.*, 2005)
	7. Taldan	K1	53.8	124.5	58.3	51.0	3.8/4.6	(*Halim et al.*, 1998a)
	8. Chulut Tsagan Del #12	K	46.1	107.5	86.5	346.5	6.9/8.8	(*Pruner*, 1992)
	9. Chulut Tsagan Del #13	K	46.1	107.5	81.0	17.2	7.7/9.7	”
	10. Gobi #14	K	46.1	107.5	72.1	211.3	6.4/8.6	”
	11. Inner Mongolia	K	44.5	118.5	82.9	249.5	5.7	(*Zhao et al.*, 1990)
Average Siberia-Amuria		*K1-K2*	*48.1*	*110.6*	*86.4*	*191,1*	*n = 10, k = 74.9, A95 = 5.8°*	

Note: Slat, Slon (Plat, Plon): Latitude and longitude of sites (paleopoles); dp/dm: half-angles of ellipse of confidence; A_{95}: radius of 95% cone of confidence; NCB (SCB): North (South) China Block; Numbers before locality names refer to numbers quoted in Fig. 6.

of a low coercivity mineral. The high temperature susceptibility measurement (Fig. 4d) displays a sharp drop in the susceptibility around 550 °C, similar to the Curie point of titanomagnetite with ∼5 per cent titanium. Other specimens display lower Curie points at 350–400 °C, corresponding to ∼30–40 per cent of titanium. All these observations lead us to conclude that Pseudo-single domain (PSD) (Fig. 4e) titanomagnetite recorded the primary magnetization for these 27 effusive edifices and basaltic lava flows.

The overall HTC *in situ* mean palaeomagnetic direction for this volcanic area (Table 3, Fig. 5) is $D = 12.1°$, $I = 66.4°$ ($n = 27$, $k = 53.0$, $\alpha_{95} = 3.9°$). No fold test is to be performed on these data because the underlying red sediments are flat-lying, we therefore, consider that any local tilt of flows results from emplacement, and not from tectonic processes. Directions exhibit normal polarity, which is consistent with an age of flow emplacements within the CLNS. Note that five site-mean directions appear as outliers (plus symbols, and the thin great-circle of site 97 in Fig. 5) and have been excluded from the final mean calculation. Albeit very close, this overall mean (white star, Fig. 5) is distinct from the IGRF field computed for summer 2004 in the location (grey diamond, Fig. 5), and the dipole field direction (grey star).

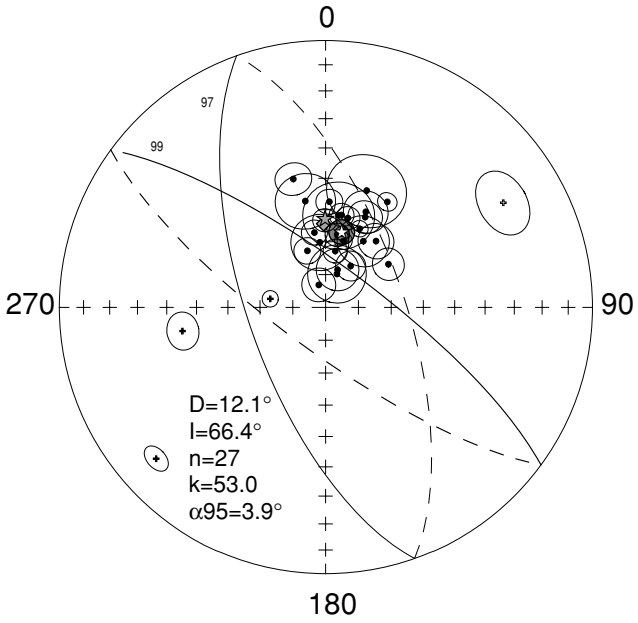

Figure 5. Equal-area projection of Arts-Bogd HTC site-mean directions, with their α_{95} circles of confidence; bold (light) continuous line: average remagnetization great-circle of site 99 (97); white star with shaded α_{95} area: overall-mean direction; plus symbols and light grey great-circle: sites excluded from the final mean direction calculation; grey diamond (star): International Geomagnetic Reference Field (Dipolar Field) direction. Same conventions as in Fig. 3.

Based on the 26 distinct flows of Table 2 (excluding the average great-circle of site 99), we obtain a VGP scatter of 14.8°, which falls not far from the 14.9°–19.5° range of VGP scatter predicted for 40–50° latitude during the 80–110 Ma period (McFadden *et al.* 1991). This suggests that the overall mean direction of HTC from our 27 basalt flows from Arts-Bogd have fully averaged out the secular variation by the time of flow-emplacement. Therefore, the final mean direction (Table 2) represents the Late Cretaceous time-averaged palaeomagnetic field direction in the 98.2–118.3 Ma time period (average value: 104.5 ± 7.1 Ma, after our results in Table 1).

4 PALAEOPOLES—DISCUSSION

From the results of K–Ar dating and palaeomagnetic analysis given above, we propose two new Cretaceous palaeopoles for the Amuria block (Table 3, Fig. 6). The first one, based on Shovon and Khurmen Uul data, lies at $\lambda = 84.7°$N, $\phi = 195.0°$ ($dp/dm = 5.8/7.5$), yielding a Late Cretaceous (Cenomanian/Turonian) palaeolatitude for the Shovon-Khurmen Uul area of 44.1° ± 5.8°N. From our 94.7 ± 1.3 Ma K–Ar dating of Shovon, and the 92.0 ± 4.0 Ma age of Khurmen Uul (Yarmolyuk *et al.* 1995), we propose that this pole is characteristic of the Amuria block at 93.4 ± 2.6 Ma.

For the Arts-Bogd locality, the age is less well constrained. In effect, our K–Ar experiments revealed ages spanning a ∼20 Ma period, from 98.2 to 118.3 Ma. Only a complete radiometric dating of the 32 flows we sampled would help gain a finer level of analysis. From our data, we compute a mean palaeopole for Arts-Bogd from the whole population of Table 2, to which we assign an average age based on our five age determinations (Table 1). This palaeopole is located at $\lambda = 80.5°$N, $\phi = 159.0°$E ($dp/dm = 5.2/6.3$), leading to

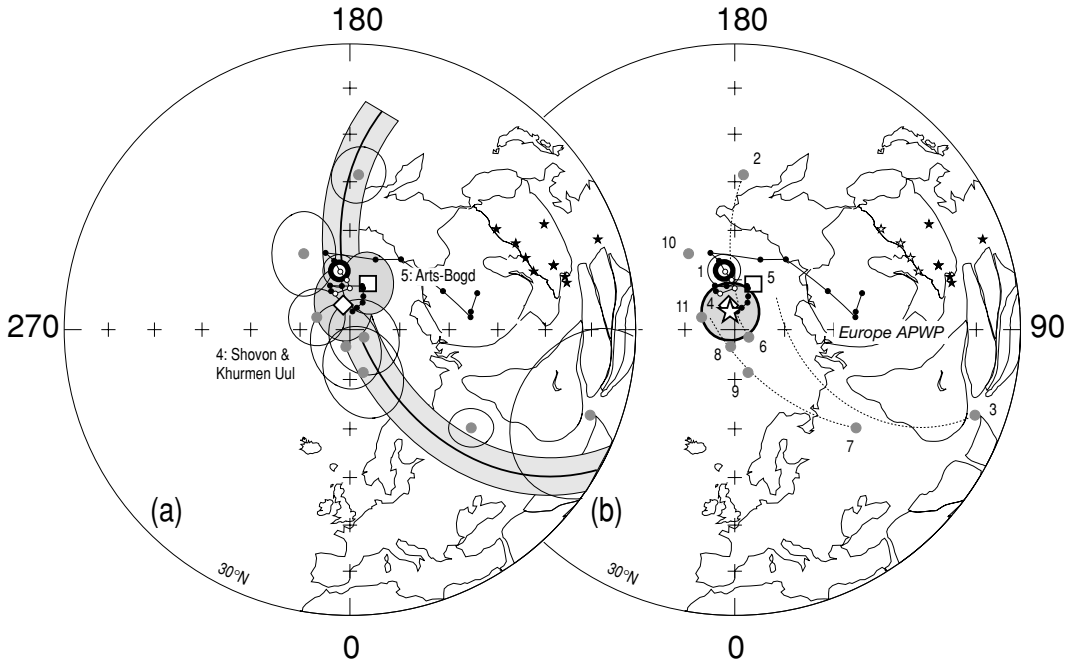

Figure 6. Equal-area projections of palaeomagnetic poles in the Earth's northern hemisphere; white diamonds: Shovon-Khurmen Uul palaeopole; white squares: Arts-Bogd palaeopole; grey dots: coeval palaeopoles from Siberia and Amuria; large white dot: NCB+SCB after Halim *et al.* (1998b); small linked dots: reference APWP poles for Europe (Besse & Courtillot 2002, 2003); white small dots: reference poles at 90, 100, 110 and 120 Ma; black and white small stars: site locations; light grey area with bold black line in (a): small-circle with its 95 per cent confidence area passing through palaeopoles, and centred on the average site locations; dotted lines in (b): small-circles passing through individual palaeopoles, centred on the sites which are assumed to have been rotated (white stars); large white star with grey A_{95} area of confidence in (b): average mid-Cretaceous palaeopole computed from Siberia, Amuria and North China palaeopoles; numbers 1–11 in (b): palaeopole numbers as given in Table 3.

a palaeolatitude position of Arts-Bogd locality at 48.9 ± 5.2°, and is thought to characterize the Cretaceous (Albian) position of the Amuria block at 104.5 ± 7.1 Ma.

Our two poles from Shovon-Khurmen Uul, based on 23 distinct flows, and Arts-Bogd, based on 27 distinct flows are shown in Fig. 6. At first sight, they do not differ from one another, and the Shovon-Khurmen Uul pole dp/dm area of confidence contains the present-day North Pole. However, they are based on a high, stable unblocking temperature magnetization carried by magnetite, which we assume to be the primary mid-Cretaceous magnetization. In effect, they do not show any significant discrepancy in either palaeolatitude or rotation with respect to the corresponding reference APWP poles for Europe at 90, 100, 110 and 120 Ma (Besse & Courtillot 2002, 2003). In terms of tectonic movement, this consistency can be interpreted as a lack of convergence between these Mongolian areas with respect to Siberia since at least 120 Ma on the one hand, and no local rotations under the effect of neotectonic deformation in the region on the other hand. This conclusion, which contradicts our first analysis and interpretation of Khurmen Uul results based on 6 flows (Hankard *et al.* 2005), is consistent with previous hypotheses (e.g. Enkin *et al.* 1992; Chen *et al.* 1993; Halim *et al.* 1998b), studies from the Amuria block (Zhao *et al.* 1990; Pruner 1992) and studies from the Mongol-Okhotsk suture zone (Halim *et al.* 1998a; Kravchinsky *et al.* 2002; Cogné *et al.* 2005).

When compared to previously published coeval poles from Siberia and Mongolia (Table 3, grey dots in Fig. 6a), reported by Zhao *et al.* (1990), Pruner (1992), Halim *et al.* (1998a), Cogné *et al.* (2005), our poles (poles number 4 and 5, Table 3, Fig. 6) are not statistically different from Ingoda River and Bichura poles (numbers 2 and 3, from north of the Mongol-Okhotsk suture zone in Siberia), Kremljevka pole (number 6, from south of the Mongol-Okhotsk suture zone in Amuria Block; (Cogné *et al.* 2005), and Taldan pole (number 7, from Amuria Block; Halim *et al.* 1998a). When compared to the Chulut Tsagan Del #12, Chulut Tsagan Del #13 and Gobi #14 poles (numbers 8, 9 and 10, respectively, Table 3) of Pruner (1992) from Mongolia, and to the Inner Mongolia pole (number 11) of Zhao *et al.* (1990), our poles do not show any palaeolatitudinal discrepancy either. This is illustrated by the small-circle one can draw over these poles (Fig. 6a), centred on the average site location (48.1°N/110.6°E), which suggests that Amuria has not experienced any relative latitudinal displacement with respect to Siberia since at least the Early Cretaceous. This analysis corroborates the generally accepted conclusion that the South China Block, North China Block and Amuria block have formed a rigidly attached unit since their accretion to Siberia by the Late Jurassic–Early Cretaceous (Zhao & Coe 1987; Zhao *et al.* 1990; Enkin *et al.* 1992; Chen *et al.* 1993; Ma *et al.* 1993; Gilder *et al.* 1996; Gilder & Courtillot 1997; Halim *et al.* 1998a,b; Yang & Besse 2001; Yang *et al.* 2001; Kravchinsky *et al.* 2002; Cogné *et al.* 2005).

As a final point, we attempt to propose a reference average palaeopole during the Cretaceous (at the limit of the Early/Late Cretaceous) for the Siberia and Amuria blocks. Based on the analysis of the small-circle distribution of palaeopoles from the Mongol-Okhotsk suture zone as proposed by Cogné *et al.* (2005), we have computed an average palaeopole, using data from Table 3, as a mixed average of fixed data from Amuria block, and small-circles passing through palaeopoles from the suture zone (Fig. 6b), excluding the pole from NCB+SCB (number 1 in Table 3). This mean palaeopole for Siberia and Amuria (Table 3, white star in Fig. 6b) lies at: 86.4 °N, 191.1°E ($n = 10$; $k = 74.9$; $A_{95} = 5.8°$). The angular distance

between this average pole and reference poles from Europe APWP is insignificant, 4.8° ± 8.9° at 100 Ma, and amounts to 6.4° ± 7.2° at 110 Ma. For a reference point situated at the average site location (48.1°N, 110.6°E), these distances translate into a component of counterclockwise rotation of the average locality of Rot = −6.9° ± 13.7° and Rot = − 9.6° ± 10.9° and to an insignificant far-sided offset of poles of $\Delta\lambda = 1.8° \pm 7.1°$ and $\Delta\lambda = 1.5° \pm 5.7°$, at 100 and 110 Ma, respectively. The same analysis holds for the comparison of our Siberia-Amuria new pole with the average NCB+SCB pole as proposed by Halim *et al.* (1998b). The angular distance between the two poles (8.4° ± 6.7°) results from a relative CCW rotation of Rot = −12.7° ± 10.1° of our new pole with respect to the NCB+SCB one, and an unsignificant palaeolatitude offset of $\Delta\lambda = 0.3° \pm 5.3°$. The CCW rotation of the mean pole is thought to be an unimportant feature due to the local rotations at each locality and the way we computed the average. Importantly, this analysis shows that the mid-Cretaceous (∼90–120 Ma) part of Europe APWP is consistent with the palaeolatitude of Siberia and Amuria at that time, itself consistent with North and South China palaeolatitudes. This reinforces the idea that this APWP can be used as a reference for studying the post-Cretaceous motion and rotation of Asian blocks with respect to Siberia.

5 CONCLUSION

We have reported new palaeomagnetic results from 61 sites (20 from Shovon, seven from Khurmen Uul, and 34 from Arts-Bogd) of Cretaceous basalt flows and volcanic edifices collected in the Gobi Desert of Mongolia. Both AF and thermal demagnetization processes isolated a stable primary normal polarity magnetization component, consistent with the age of emplacement of these basalts during the Long Normal Cretaceous Superchron. Rock magnetism experiments confirmed that HTC is carried by magnetite (Shovon and Khurmen Uul region) and titanomagnetite (Arts-Bogd). K–Ar datings allow us to propose a 94.7 ± 1.3 Ma age for Shovon locality and a 98.2 ± 1.4 to 118.3 ± 1.7 Ma age range for Arts-Bogd. We have computed 2 new palaeopoles, one based on including both palaeomagnetic results from the Shovon and Khurmen Uul localities (average age: 93.4 ± 2.6 Ma), the other based on the HTC from Arts-Bogd (average age: 104.5 ± 7.1 Ma). Notwithstanding the large local rotations of some coeval poles evidenced from the small-circle distribution of poles from Siberia, Amuria and North China blocks, our two new mid-Cretaceous poles are consistent with the corresponding reference poles from Europe APWP. This implies the lack of any relative latitudinal displacement between Amuria block and Siberia since at least the end of Early Cretaceous. This concordance also agrees with the generally accepted assumption that the South China Block, North China block and Amuria have been rigidly attached since the Late Jurassic–Early Cretaceous. These well-dated new data fill a gap in Cretaceous data between the Mongol-Okhotsk suture to the north, and North China Block to the south.

ACKNOWLEDGMENTS

This study is part of cooperation between IPGP and The Mongolian University of Science and Technology. We thank Mongolian staff, in particular Uyanga, Khatna and Moogii, for their efficiency in conducting the 2004 field trip to Gobi Desert. An early draft of this paper benefited from kind and helpful comments and suggestions from V. Courtillot, A. Jay and J. Hernlund. This is IPGP contribution 2181.

REFERENCES

Besse, J. & Courtillot, V., 1991. Revised and Synthetic Apparent Polar Wander Paths of the African, Eurasian, North American and Indian Plates, and True Polar Wander Since 200 Ma, *J. Geophys. Res.,* **96,** 4029–4050.

Besse, J. & Courtillot, V., 2002. Apparent and true polar wander and the geometry of the geomagnetic field over the last 200 Myr, *J. Geophys. Res.,* **107,** 1–31.

Besse, J. & Courtillot, V., 2003. Correction to Apparent and true polar wander and the geometry of the geomagnetic field in the last 200 Myr, *J. Geophys. Res.,* **108,** 2469 doi:10.129/2003JB002684.

Cande, S.C. & Kent, D.V., 1995. Revised calibration of the geomagnetic polarity timescale for the Late Cretaceous and Cenozoic, *J. Geophys. Res.,* **100,** 6093–6095.

Cassignol, C. & Gillot, P.-Y., 1982. Range and effectiveness of unspiked potassium-argon dating, in *Numerical Dating in Stratigraphy*, pp. 159–172, ed. Odin G.S., Wiley Publication, Chichester.

Chen, Y., Cogné, J.P., Courtillot, V., 1992. New Cretaceous paleomagnetic poles from the Tarim Basin, northwestern China, *Earth planet. Sci. Lett.,* **114,** 17–38.

Chen, Y., Courtillot, V., Cogné, J.-P., Besse, J., Yang, Z. & Enkin, R., 1993. The Configuration of Asia prior to the Collision of India: cretaceous paleomagnetic constraints, *J. Geophys. Res.,* **98,** 21 927–21 941.

Cogné, J.P., 2003. PaleoMac: a Macintosh™ application for treating paleomagnetic data and making plate reconstructions, *Geochem. Geophys. Geosyst.,* Paris.

Cogné, J.P., Kravchinsky, V., Halim, N. & Hankard, F., 2005. Late Jurassic-Early Cretaceous closure of the Mongol-Okhotsk Ocean demonstrated by new Mesozoic paleomagnetic results from the Trans-Baïkal area SE Siberia, *Geophys. J. Int.,* **163,** 813–832.

Day, R., 1977. TRM and its Variation with Grain Size, *J. Geomag. Geoelectr.,* **29,** 233–265.

Enkin, R.J., Yang, Z., Chen, Y. & Courtillot, V., 1992. Paleomagnetic Constraints on the Geodynamic History of the Major Blocks of China From the Permian to the Present, *J. Geophys. Res.,* **97,** 13 953–13 989.

Fisher, R.A., 1953. Dispersion on a sphere, *Proc. Soc. Lond., Ser. A,* **217,** 295–305.

Gilder, S. & Courtillot, V., 1997. Timing of North-South China collision from new middle to Late Mesozoic paleomagnetic data from the North China Block, *J. Geophys. Res.,* **102,** 17 713–17 727.

Gilder, S. *et al.*, 1996. Isotopic and paleomagnetic constraints on the Mesozoic tectonic evolution of South China, *J. Geophys. Res.,* **101,** 16 137–16 154.

Gilder, S.A., Chen, Y., Cogné, J.-P., Tan, X., Courtillot, V., Sun, D. & Li, Y., 2003. Paleomagnetism of Upper Jurassic to Lower Cretaceous volcanic and sedimentary rocks from the western Tarim Basin and implications for inclination shallowing and absolute dating of the M-O (ISEA?) chron, *Earth planet. Sci. Lett.,* **206,** 587–600.

Gillot, P.-Y. & Cornette, Y., 1986. The Cassignol technique for potassium-argon dating, precision and accuracy: examples from the late Pleistocene to recent volcanics from southern Italy, *Chem. Geol. (Isotope Geoscience section),* **59,** 205–222.

Gillot, P.-Y., Cornette, Y. & Max, N., 1992. Two reference materials, trachytes MDO-G and ISH-G, for argon dating (K–Ar and 40Ar/39Ar) of Pleistocene and Holocene Rocks, *Geostandards, Newslett.,* **16**(1), 55–60.

Gradstein, F.M., Ogg, J.G., Smith, A.G. *et al.*, 2004. *A geologic Time Scale 2004*, 589 pp., Cambridge University Press.

Halim, N., Kravchinsky, V., Gilder, S., Cogné, J.P., Alexyutin, M., Sorokin, A., Courtillot, V. & Chen, Y., 1998a, A paleomagnetic study from the Mongol-Okhotsk region: rotated Early Cretaceous volcanics and remagnetized sediments, *Earth planet. Sci. Lett.,* **159,** 133–145.

Halim, N., Cogné, J.P., Chen, Y., Atasiei, R., Besse, J., Courtillot, V., Gilder, S., Marcoux, J. & Zhao, R.L., 1998b, New Cretaceous and Early Tertiary paleomagnetic results from Xining-Lanzhou basin, Kunlun and Qiangtang blocks, China: implications on the geodynamic evolution of Asia, *J. Geophys. Res.,* **103**(B9), 21 025–21 045.

Halls, H.C., 1978. The use of converging remagnetization circles in paleomagnetism, *Phys. Earth planet. Inter.,* **16,** 1–11.

Hankard, F., Cogné, J.-P. & Kravchinsky, V., 2005. A new Late Cretaceous paleomagnetic pole for the west of Amuria block (Khurmen Uul, Mongolia), *Earth planet. Sci. Lett.,* **236,**(1–2), 359–373.

Kirshvink, J.L., 1980. The least-squares line and plane and the analysis of paleomagnetic data, *Geophys. J.R. astr. Soc.,* **60,** 699–718.

Koenigsberger, J.G., 1938. Natural residual magnetism of eruptive rocks, *Terr. Magn. Atmos. Elect.,* **43,** 119–130, 299–320.

Kovalenko, D.V., Yarmolyuk, V.V. & Solov'ev, A.V., 1997. Migration of volcanic centers of the south Khangai hot spot : paleomagnetic evidence, *Geotectonics,* **31,** 228–235.

Kravchinsky, V.A., Cogné, J.P., Harbert, W. & Kuzmin, M.I., 2002. Evolution of the Mongol–Okhotsk Ocean as constrained by new palaeomagnetic data from the Mongol–Okhotsk suture zone, Siberia, *Geophys. J. Int.,* **148,** 34–57.

Le Goff, M., 1990. Lissage et limites d'incertitude des courbes de migration polaire; pondération des données et extension bivariate de la statistique de Fisher, *C. R. Acad. Sci. Paris,* **311**(II), 1191–1198.

Ma, X., Yang, Z. & Xing, L., 1993. The Lower Cretaceous reference pole for north China, and its tectonic implications, *Geophys. J. Int.,* **115,** 323–331.

McFadden, P.L. & McElhinny, M.W., 1988. The combined analysis of remagnetization circles and direct observations in paleomagnetism, *Earth planet. Sci. Lett.,* **87,** 161–172.

McFadden, P.L., Merill, R.T., McElhinny, M.W. & Sunhee, L., 1991. Reversal of the Earth's magnetic field and temporal variations of the dynamo families, *J. Geophys. Res.,* **96,** 3923–3933.

Molnar, P. & Tapponnier, P., 1975. Cenozoic tectonics of Asia: effects of a continental collision, *Science.,* **189,** 419–426.

Odin, G.S. *et al.*, 1982, Interlaboratory standards for dating purposes, in *Numerical Dating in Stratigraphy*, pp. 123–150, ed. Odin, G.S., Wiley, Chichester.

Patriat, P. & Achache, J., 1984. India-Eurasia collision chronology has implications for crustal shortening and driving mechanism of plates, *Nature,* **311,** 615–621.

Pruner, P., 1992. Paleomagnetism and paleogeography of Mongolia from the Carboniferous to Cretaceous—final report, *Phys. Earth planet. Inter.,* **70,** 169–177.

Quidelleur, X., Gillot, P.-Y., Soler, V. & Lefèvre, J.C., 2001. K-Ar dating extended into the last millennium: application to youngest effusive episode of the Teide volcano (Spain), *Geophys. Res. Lett.,* **28,** 3067–3070.

Steiger, R.H. & Jaeger, E., 1977. Subcommission on geochronology: convention on the use of decay constants in geo- and cosmochronology, *Earth planet. Sci. Lett.,* **36,** 359–362.

Tapponnier, P. & Molnar, P., 1979. Active faulting and cenozoic tectonics of Tien Shan, Mongolia, and Baykal regions, *J. eophys. Res.,* **84,** 3425–3459.

Tapponnier, P., Peltzer, G. & Armijo, R., 1986. On the mechanics of the collision between India and Asia, *Geol. Soc. Spec. Publ.,* **19,** 115–157.

Whitford-Stark, J.L., 1987. A survey of cenozoic volcanism on mainland Asia, *Geol. Soc. Am., Special paper,* **213,** 20–23.

Yang, Z. & Besse, J., 1993. Paleomagnetic study of Permian and mesozoic sedimentary rocks from Northern Thailand supports the extrusion model for Indochina, *Earth planet. Sci. Lett.,* **117,** 525–552.

Yang, Z. & Besse, J., 2001. New Mesozoic apparent polar wander path for south China: tectonic consequences, *J. Geophys. Res.,* **106,** 8493–8520.

Yang, Z., Yin, J., Otofuji, Y.I. & Sato, K., 2001. Discrepant Cretaceous paleomagnetic poles between Eastern China and Indochina: a consequence of the extrusion of Indochina, *Tectonophysics,* **334,** 101–113.

Yarmolyuk, V.V., Ivanov, V.G., Samoylov, V.S. & Arakelianst, M.M., 1995. Formation stages of Mesosoic and Cenozoic intraplate volcanism of South Mongolia, *Doklady Academii Nauk,* **344**(5), 673–676 (In Russian).

Yarmolyuk, V.V., Kovalenko, D.V., Sal'nikova, E.B., Budnikov, S.V., Kovach, V.P., Kotov, A.B. & Ponomarchuk, V.A., 2002. Tectono-Magmatic zoning, Magma sources, and Geodynamics of the Early Mesozoic Mongolia-Transbaikal Province, *Geotectonics,* **36,** 42–63.

Zhao, X. & Coe, R.S., 1987. Paleomagnetic constraints on the collision and rotation of North and South China, *Nature,* **327,** 141–144.

Zhao, X., Coe, R.S., Zhou, Y., Wu, H. & Wang, J., 1990, New paleomagnetic results from northern China: collision and suturing with Siberia and Kazakstan, *Tectonophysics,* **181,** 43–81.

Zonenshain, L.P., Kuzmin, M.I. & Moralev, V.M., 1990. Geology of the USSR: a plate tectonic synthesis, *Geodynamics Series,* Vol. 21, AGU, Washington DC, p. 242.

Zijderveld, J.D.A., 1967, A.C. demagnetization of rocks: analysis of results, in *Methods in Paleomagnetism*, pp. 254–286, eds Collinson, D.W., Creer, K.M. & Runcorn, S.K., Elseiver, New York.